Computationally efficient thermal-mechanical modelling of selective laser melting

Yang, Yabin; Ayas, Can

DOI
10.1063/1.5008031

Publication date
2017

Document Version
Final published version

Published in
Proceedings of the 20th International ESAFORM Conference on Material Forming (ESAFORM 2017)

Computationally efficient thermal-mechanical modelling of selective laser melting

Yabin Yang, and Can Ayas

Citation: AIP Conference Proceedings **1896**, 040005 (2017);
View online: https://doi.org/10.1063/1.5008031
View Table of Contents: http://aip.scitation.org/toc/apc/1896/1
Published by the American Institute of Physics

Computationally Efficient Thermal-Mechanical Modelling of Selective Laser Melting

Yabin Yang[1,b)] and Can Ayas[1,a)]

[1]*Structural Optimization and Mechanics Group, Department of Precision and Microsystems Engineering, Faculty of Mechanical, Maritime and Material Engineering, Delft University of Technology, Mekelweg 2, 2628 CD, Delft, The Netherlands*

[a)]Corresponding author: C.Ayas@tudelft.nl
[b)]Y.Yang-6@tudelft.nl

Abstract. The Selective laser melting (SLM) is a powder based additive manufacturing (AM) method to produce high density metal parts with complex topology. However, part distortions and accompanying residual stresses deteriorates the mechanical reliability of SLM products. Modelling of the SLM process is anticipated to be instrumental for understanding and predicting the development of residual stress field during the build process. However, SLM process modelling requires determination of the heat transients within the part being built which is coupled to a mechanical boundary value problem to calculate displacement and residual stress fields. Thermal models associated with SLM are typically complex and computationally demanding. In this paper, we present a simple semi-analytical thermal-mechanical model, developed for SLM that represents the effect of laser scanning vectors with line heat sources. The temperature field within the part being build is attained by superposition of temperature field associated with line heat sources in a semi-infinite medium and a complimentary temperature field which accounts for the actual boundary conditions. An analytical solution of a line heat source in a semi-infinite medium is first described followed by the numerical procedure used for finding the complimentary temperature field. This analytical description of the line heat sources is able to capture the steep temperature gradients in the vicinity of the laser spot which is typically tens of micrometers. In turn, semi-analytical thermal model allows for having a relatively coarse discretisation of the complimentary temperature field. The temperature history determined is used to calculate the thermal strain induced on the SLM part. Finally, a mechanical model governed by elastic-plastic constitutive rule having isotropic hardening is used to predict the residual stresses.

INTRODUCTION

Additive manufacturing (AM) is a unique way of building three-dimensional objects in a layer by layer fashion, resulting in a excellent ability of building complex products with few manufacturing constraints. Selective laser melting (SLM) is the most common AM technique suitable for producing metal parts. In SLM, metal powder is fully melted with a focused laser beam and therefore the final product can achieve a density which is 99.9% of its theoretical density [1]. Mechanical properties of SLM products are also similar to those of produced by conventional manufacturing techniques [1, 2]. However, in order to make high quality and high precision parts, distortion of the part during the built should be minimum. Consequently, a considerable effort is spent to identify the process parameters, such as the laser power, scanning speed and scanning pattern ensuring the minimum distortion of the part. Otherwise, part distortions which arise due to the thermal gradients can disqualify parts with low dimensional tolerances or the associated residual stresses can lead to part failure, delamination or cracking. It is time consuming and expensive to experimentally identify suitable process parameters. Consequently, numerical methods such as the finite elements (FE) and finite differences (FD) are widely used by the scientific community to study the influence of the process parameters on the end product quality[3, 4].

Process simulation of the SLM process using above mentioned standard numerical methods require a fine numerical discretisation both in space and time in order to resolve heating with a laser spot which is typically tens of micrometers. This in turn makes the model computationally intractable. Therefore, the objective of the present paper is to develop a computationally efficient thermal-mechanical model for predicting the residual stresses and part

Proceedings of the 20th International ESAFORM Conference on Material Forming
AIP Conf. Proc. 1896, 040005-1–040005-6; https://doi.org/10.1063/1.5008031
Published by AIP Publishing. 978-0-7354-1580-5/$30.00

distortions of an SLM product. A semi-analytical thermal model is first described to determine the temperature evolution of the part. In this model the effect of laser is described using an analytical solution of the line heat sources in a semi-infinite medium which is corrected for the actual boundary conditions with a complimentary temperature field. The complimentary temperature field is deduced from the solution of a boundary value problem (BVP) using finite difference (FD) method. Subsequently, temperature field at a given time instance is used as an in input for the mechanical model giving rise to thermal strains. A temperature dependent elastic-plastic constitutive relation is used to predict part distortions and residual stresses.

MODEL DESCRIPTION

Consider a three dimensional body V that has already been built and a thin layer of powder is laid on its top surface ∂V_{top}, as shown in Fig. 1a. The lateral surface ∂V_{lat} is covered by the powder while the bottom surface ∂V_{bot} is bonded to the base plate. The coordinate system is shown in Fig. 1b. At time $t = 0$ the laser starts to scan over the uppermost powder layer where a single scan vector having an angle θ with the x_1 axis is applied as shown in Fig. 1b. In response the temperature of the body V increase as dictated by heat equation

$$\rho c_p \frac{\partial T}{\partial t} = \nabla.(k\nabla T) + Q_v, \qquad \text{in} \quad V, \tag{1}$$

where T is the temperature, Q_v is the rate of volumetric heat generation, i.e. the source term, ρ, c_p and k are the density, the constant-pressure specific heat and the thermal conductivity, respectively. As the mean conductivity of the powder covering ∂V_{lat} and ∂V_{top} is approximately hundred times smaller than that of the solid body [5], it is justified to assume that the powder has negligible heat conductivity. Moreover, the amount of heat lost due to radiation and convection from the top surface ∂V_{top} is also negligible in comparison to the amount of heat transferred by conduction to the interior of the solid body [6, 7]. As a result, no heat-flux boundary condition is applied on the lateral and top surfaces ∂V_{lat} and ∂V_{top}, respectively. During the SLM process typically the temperature of the baseplate is kept at a constant value. Therefore the bottom surface ∂V_{bot} is set to be at a fixed temperature.

If the material parameters ρ, c_p and k are assumed to be temperature independent, Eq. (1) becomes the linear heat equation and can be solved using the superposition principle. First, the laser scanning line is described by a finite number of point heat sources, as shown in Fig. 1a. The temperature due to a single point source in an semi-infinite space (the boundary of the semi-infinite space coincides with ∂V_{top}) can be expressed by [8]

$$\tilde{T}_p(x_i, t) = \frac{QA}{4\rho c_p \left(\pi\alpha\,(t - t_0 + t_r)\right)^{3/2}} \exp\left(\frac{-R^2}{4\alpha(t - t_0 + t_r)}\right) \tag{2}$$

where Q represents the energy associated with the heat source while the absorptivity A is determined as detailed in [7]. The thermal diffusivity $\alpha = k/\rho c_p$. Time t_0 marks the activation instance of the source and the time shift $t_r = r_l^2/8\alpha$ is used to eliminate the singularity at $t = t_0$. The expression t_r implies the point source has diffused a distance r_l, which is equal to the spot radius of the laser. The distance between the material point of interest x_i and the point source position is represented by R. If the number of point sources representing a scanning line is sufficiently high, the energy Q given in Eq.(2) can be represented by $Q = P\Delta t$, where P is the power of the laser, and Δt is the time step.

In order to construct a line heat source, we consider the limiting case of infinitely many point sources along the scanning direction. The temperature field $\tilde{T}_L$ due to a scanning line is then computed as a line heat source that can be obtained by the integration of Eq. (2) over time

$$\tilde{T}_L(x_i, t_f) = \frac{PA}{4\rho c_p(\pi\alpha)^{3/2}} \int_0^{t_f} \frac{\exp\left(-\frac{R^2}{4\alpha(t_f - t + t_r)}\right)}{(t_f - t + t_r)^{3/2}} \mathrm{d}t, \tag{3}$$

where t_f is the time instance of interest. Eq.(3) can be cast into a closed form, which is given in Appendix A.

Finally the total temperature T can then be expressed as the superposition of the temperature field denoted by $\tilde{T}_L$ and the complementary field $\hat{T}$ which enforce the boundary conditions, i.e

$$T = \tilde{T}_L + \hat{T}. \tag{4}$$

The $\hat{T}$ field can be obtained by solution of a separate boundary value problem (see [9] for details) such that the total temperature field satisfies the boundary conditions described above. An explicit finite difference scheme is used to compute $\hat{T}$ numerically. On the contrary $\tilde{T}_L$ field with the known analytical solution can capture the steep temperature gradients in the vicinity of the laser.

When a laser scanning line is applied sufficiently close to a boundary, a coarse numerical discretisation of $\hat{T}$ may not suffice. In order to avoid requiring excessive finite difference grid points, image source method, which is schematically illustrated in Fig. 1c is utilised. For a 2D problem shown in Fig. 1c with a boundary ∂B, assume that a line heat source with power P is applied close to the ∂B. In order to enforce a no-flux boundary condition on ∂B, an image source is added by mirroring the original line heat source with respect to ∂B. If image source has an energy Q equal to that of the original source, no-heat flux boundary condition on ∂B is satisfied. Moreover the solution of the image temperature field denoted by $\breve{T}$ is also given by Eq.(3). In order to avoid having excessive number of image sources the following procedure is in place. If the distance of a heat source to the boundary is greater than a critical distance, boundary conditions are enforced with $\hat{T}$ as described above.

It is important to note that the decomposition given in Eq. (4) is not unique. In the presence of image sources, Eq. (4) is modified as

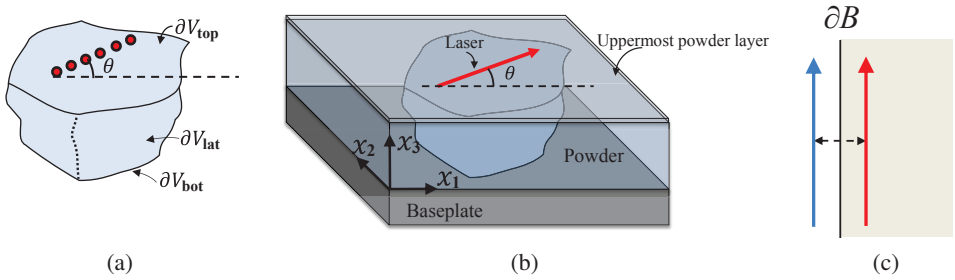

(a) (b) (c)

FIGURE 1. (a) A body V is assumed to be already built and the laser scanning line is discretised by finite number of point sources. (b) The top surface ∂V_{top} and lateral surface ∂V_{lat} are covered by the powder. (c) Schematic illustration of the image source method.

$$T = \tilde{T}_L + \breve{T} + \hat{T} \tag{5}$$

where $\breve{T}$ is the temperature field due to the image source.

Residual stress analysis

Once the temperature field T is obtained as a function of time, it can used as an input to a mechanical model to predict the residual stresses in the body V. During the SLM process, change in temperature give rise to a thermal strain field given by

$$\varepsilon_{ij}^{\text{th}} = \int_{T_{\text{ref}}}^{T} \alpha_{\text{th}}(T)\mathrm{d}T, \tag{6}$$

where α_{th} is the thermal expansion coefficient. For a material point which has not been melted during the process, the reference temperature T_{ref} in Eq. (6) is set to be the initial temperature taken as the temperature of the baseplate, while the reference temperature T_{ref} becomes the melting point if the material point has previously reached melting point. In addition to thermal strains, elastic and plastic strain fields also arise which gives a total strain field of

$$\varepsilon_{ij} = \varepsilon_{ij}^{e} + \varepsilon_{ij}^{p} + \varepsilon_{ij}^{\text{th}} \tag{7}$$

where ε_{ij}^{e} and ε_{ij}^{p} are the elastic and plastic strain tensors, respectively. Whenever a material point melts, the total strain becomes to zero. We take this phenomena into account by setting the total strain to zero when $T \geq T_m$, where T_m is the melting point. Traction free boundary conditions are applied at the boundaries ∂V_{top} and ∂V_{lat} and the base plate is taken as rigid. An elastic-plastic material model with isotropic hardening rule is used as a constitutive rule.

PROBLEM DESCRIPTION

We consider a a cuboid with the dimension of 3 mm × 3 mm × 1.56 mm which has already been built. The motivation behind the choice of dimensions is to be able to compare our results with the experimental findings and finite element calculations of Parry et al. [10] performed on this geometry. We consider building of an additional layer with a thickness of 40 μm on top of the existing body with a unidirectional scanning pattern followed by the scan of a single outer contour.

First the thermal analysis is performed. Recall that the top surface and lateral surfaces of the cuboid are insulating while the bottom surface remains at a fixed temperature which is equal to the initial temperature $T_0 = 200^oC$. Image sources are added if the distance between a line source and any lateral boundary is smaller than 1.5 mm. The time step is taken 8×10^{-5} s. The SLM processing parameters listed in Table 1 are taken from [10]. The speed for scanning the outer contour is 0.25 m/s. The thermal material properties listed in Table 2 are representative for Ti-6Al-4V at a temperature of 1400 ^oC, which is close to its melting point $T_m = 1650^o$. An 8 noded hexahedral finite difference cells with the size of 0.6 mm × 0.6 mm × 0.39 mm used to calculate the $\hat{T}$ fields.

The temperature field determined from the thermal analysis is used in the mechanical analysis as a source of thermal strain. The mechanical analysis is also performed with time intervals of $8{\times}10^{-5}$ s. The SLM part is discretised with 7803 elements. Finite element calculations are performed with the commercial code Abaqus 6.14. Young's modulus, Poisson's ratio and yield strength are taken from [10]. Both the yield strength and the isotropic hardening slope is taken to be temperature dependent. The Young's modulus and the yield strength both decrease as the temperature increases. The Poisson's ratio is 0.33. The displacement field of the cuboid calculated at a time increment is used as the initial state for the subsequent time increment. The baseplate is taken to be a rigid body in the mechanical analysis.

TABLE 1. The SLM processing parameters [10]

Laser power P **(W)**	**Laser speed** v **(m/s)**	**Laser spot radius** r **(μm)**	**Border offset (mm)**	**Hatch spacing** h **(μm/s)**	**Layer thickness (μm)**
82.5	0.5	25	0.07	90	40

TABLE 2. Material properties [10]

Conductivity k **(W/mK)**	**Heat capacity** c_p **(J/kgK)**	**Density** ρ **(g/cm^3)**	**Absorptivity** A **(-)**
26	770	4.21	0.77

RESULTS & DISCUSSIONS

The predicted melt-pool widths for the first and second tracks are predicted as 102 μm and 110 μm, receptively, which are in prefect agreement with the experimental values (104 μm and 107 μm) reported by Parry et al. [10]. In Fig. 2a the temperature history at point G located at the end of the first track, as shown in Fig. 3a is depicted. The temperature predicted by the semi-analytical model proposed in this paper and the predictions of the numerical model proposed by Parry et al.[10] both show oscillations and peak values are observed at the end of each track. After the first three tracks, the temperature predicted by the proposed model is slightly higher than that calculated by Parry [10].

Fig. 2b gives the comparison of the average temperature of the consolidated elements. Consolidated elements are the elements which have been melted and then subsequently solidified. The result shown in Fig. 2b is calculated with a uniform FD grid size of 0.02 mm, which is the same as the simulation conducted by Parry et al [10]. The two curves shown in Fig. 2b are in good agreement and they both show the same trend.

The total temperature field predicted for the layer built (3 mm × 3 mm × 0.04 mm) is then applied in the mechanical model. In Fig. 3 the residual stress and equivalent plastic strain ε^p distribution of the layer built is given when it is cooled down to the initial temperature. The total cooling time is calculated as 3 s. Scanning direction is along the x_2 axis and the scanning started from the left. Fig. 3a shows the equivalent plastic strain distribution of the top surface, while Fig. 3b and c show the stress distribution. From Fig. 3b and c, it is observed that a tensile stress

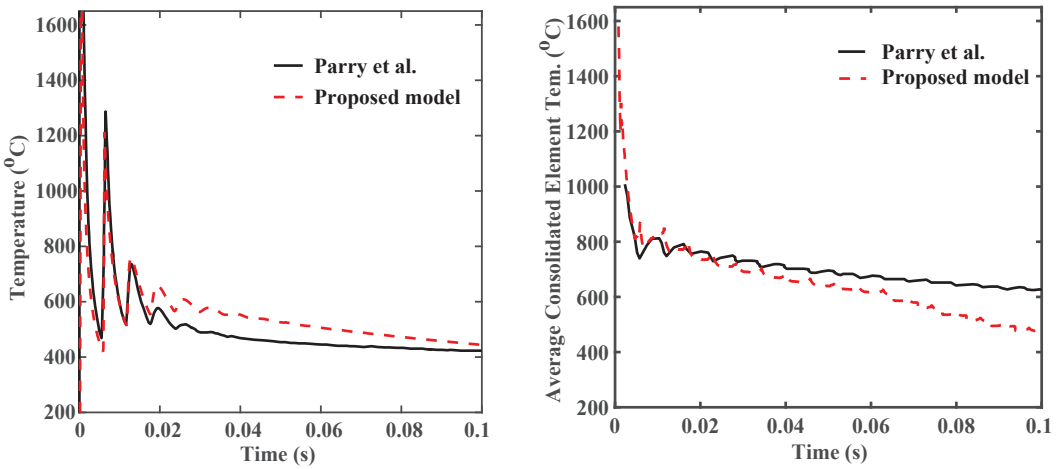

(a) (b)

FIGURE 2. Comparison between the results obtained by the proposed thermal model and the model reported by Parry et al. [10]. (a) The temperature history of point G at the end of the first track. (b) The average consolidated element temperature versus time.

state appears for most of the scanning area, which is consistent with the experimental observations[11, 12]. It can also be seen from Fig. 3 that the residual stress distribution is not uniform, but highly dependent on the scanning strategy.

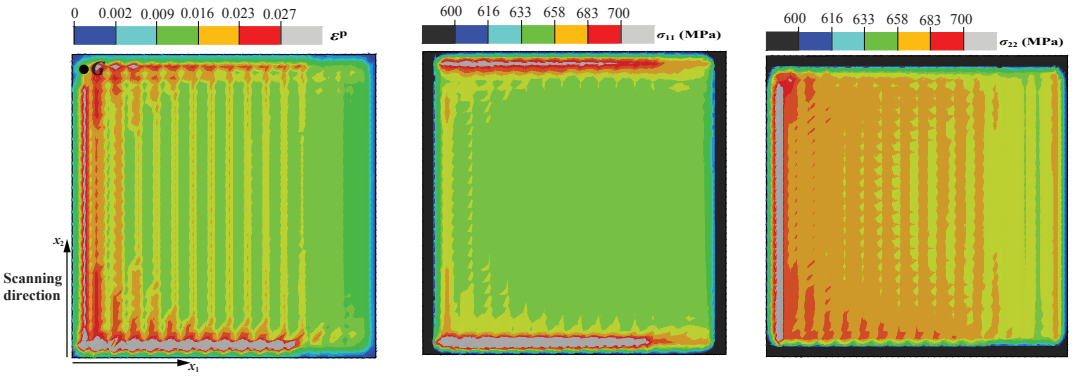

(a) (b) (c)

FIGURE 3. The Distribution of (a) equivalent plastic strain ε^{pl} and (b) stress components σ_{11}, (c) σ_{22} of the top surface.

The model described above can be easily extended for building multiple layers.Before a second layer is built, a new powder layer is recoated which takes typically around 10 seconds [13]. During the recoating period, the temperature of the solid cools down to the initial temperature. Consequently, for the thermal model, after building a layer, the modelled domain is updated by shifting the top surface ∂V_{top} with an amount equal to height of a layer, and the same initial temperature with due account is prescribed for the whole part. For the mechanical model, the geometry of the new layer is adjusted on the deformation of the previous layer. The adjusted configuration is set to be the initial state for the mechanical analysis of the subsequent layer.

CONCLUSIONS

A computationally efficient thermal-mechanical modelling approach for predicting the residual stresses during SLM process is developed. A semi-analytical model is utilized first to calculate the temperature evolution during the SLM process. The temperature field is described by the analytical solution of a line heat source representing laser scanning

and a complimentary numerical scheme accounting for the effect of the boundary conditions. Consequently, the numerical discretisation is decoupled from the laser spot dimension and hence a coarse grid can be applied in order to improve the computational efficiency of the model. The temperature field determined by the semi-analytical model is then used in a mechanical analysis to determine the residual stress.

Appendix A

Eq.(3) can be finally expressed as

$$\tilde{T}_L(x_i, t_f) = C_1 C_2 \Big(\text{erfc}(z_1) - C_3\text{erfc}(z_2) - \text{erfc}(z_3) + C_3\text{erfc}(z_4)\Big) \tag{8}$$

where $C_1 = \frac{PA}{4k\pi\sqrt{B}}$, $C_2 = \exp\left(\frac{-(\sqrt{B}+C)v_l}{2\alpha}\right)$, $C_3 = \exp\sqrt{B}v_l$, $B = R^2 - 2(x_1 - x_1^s)v_l t_f \cos\theta - 2(x_2 - x_2^s)v_l t_f \sin\theta + v_l^2 t_f^2$, $C = (x_1 - x_1^s)\cos\theta + (x_2 - x_2^s)\sin\theta - v_l t_f$, $z_1 = \frac{v_l}{2\sqrt{\alpha U}} - \frac{\sqrt{B}U}{2\sqrt{\alpha}}$, $z_2 = \frac{v_l}{2\sqrt{\alpha U}} + \frac{\sqrt{B}U}{2\sqrt{\alpha}}$, $z_3 = \frac{v_l}{2\sqrt{\alpha L}} - \frac{\sqrt{B}L}{2\sqrt{\alpha}}$, $z_4 = \frac{v_l}{2\sqrt{\alpha L}} + \frac{\sqrt{B}L}{2\sqrt{\alpha}}$, $L = (t_f + t_r)^{-1/2}$. The laser turns off at moment t_l, $U = t_r^{-1/2}$ when $t_f < t_l$, , while $U = (t_f - t_l + t_r)^{-1/2}$ when $t_f > t_l$. The starting location of the line source is x_i^s and the error function erfc(ϕ) is defined as

$$\text{erfc}(\phi) = 1 - \frac{2}{\sqrt{\pi}} \int_{\phi}^{\infty} \exp(-\xi^2)\text{d}\xi \tag{9}$$

REFERENCES

[1] B. Vandenbroucke and J. P. Kruth, Rapid Prototyping Journal **11**, 26–36 (2007).

[2] C. Casavola, S. L. Campanelli, and C. Pappalettere, The Journal of Strain Analysis for Engineering Design **44**, 93–104 (2009).

[3] N. E. Hodge, R. M. Ferencz, and J. M. Solberg, Computational Mechanics **54**, 33–51 (2014).

[4] M. F. Zaeh and G. Branner, Production Engineering **4**, 35–45 (2010).

[5] A. V. Gusarov, I. Yadroitsev, P. Bertrand, and I. Smurov, Journal of Heat Transfer **131**, p. 072101 (2009).

[6] I. Roberts, C. Wang, R. Esterlein, M. Stanford, and D. Mynors, International Journal of Machine Tools and Manufacture **49**, 916–923 (2009).

[7] A. Robert and Debroy, Metallurgical and Materials Transactions B **32**, 941–947 (2001).

[8] H. Carslaw and J. Jaeger, in *Conduction of Heat in Solids* (Oxford Science Publications, 1959).

[9] Y. Yang, M. F. Knol, F. Keulen, and C. Ayas, A Semi-Analytical Thermal Modelling Approach for Selective Laser Melting **submitted for publication**.

[10] L. Parry, I. A. Ashcroft, and R. D. Wildman, Addtive Manufacturing **12**, 1–15 (2016).

[11] P. Mercelis and J. P. Kruth, Rapid Prototyping Journal **12**, 254–265 (2006).

[12] M. Shiomi, K. Osakada, K. Nakamura, T. Yamashita, and F. Abe, CIRP Annals-Manufacturing Technology **53**, 195–198 (2004).

[13] L. Papadakis and A. Loizou, "A thermo-mechanical modeling reduction approach for calculation shape distortion in slm manufacturing for aeroengine components," in *International Conference on Advanced Research in Virtual and Rapid Prototyping* (2013), pp. 613 – 618.